International Journal of Solids and Structures 243 (2022) 111525

Contents lists available at ScienceDirect

International Journal of Solids and Structures

journal homepage: www.elsevier.com/locate/ijsolstr

Correlation between slip precursors and topological length scales at the onset of frictional sliding

Gianluca Costagliola [a], Federico Bosia [b], Nicola M. Pugno [c,d,*]

[a] Civil Engineering Institute, École Polytechnique Fédérale de Lausanne - EPFL, 1015 Lausanne, Switzerland
[b] DISAT, Politecnico di Torino, Corso Duca degli Abruzzi 24, 10129 Torino, Italy
[c] Laboratory for Bioinspired, Bionic, Nano, Meta Materials & Mechanics, Department of Civil, Environmental and Mechanical Engineering, University of Trento, Via Mesiano 77, 38123 Trento, Italy
[d] School of Engineering and Materials Science, Queen Mary University of London, Mile End Road, London E1 4NS, UK

ARTICLE INFO

Keywords:
Friction
Multiscale structures
Slip precursors
Numerical simulations

ABSTRACT

Understanding the interplay between concurrent length scales is a fundamental issue in many problems involving friction between sliding interfaces, from tribology to the study of earthquakes and seismic faults. On the one hand, a macroscopic sliding event is preceded by slip precursors with a characteristic propagation length scale. On the other hand, the emergent frictional properties can be modified by surface patterning depending on their geometric length scale. This suggests that macroscopic sliding of structured surfaces is governed by the interplay between the length scale of the slip precursors and those characterizing the geometric features. In this paper, we investigate these aspects by means of numerical simulations using a two-dimensional spring-block model. We discuss the influence of the geometric features on the occurrence and localization of slip precursors, extending the study to interfaces characterized by two geometric length scales. We find that different types of detachment sequences are triggered by specific surface structures, depending on their scales and relation to sliding direction, leading to a macroscopically smooth transition to sliding in the case of hierarchical and/or anisotropic features. These concepts could be exploited in devices switching from static to dynamic sliding, and can contribute to an improvement in the understanding and interpretation of seismic data.

1. Introduction

The onset of frictional sliding motion between two dry surfaces displays an intriguing interplay of effects that have been investigated in many recent works. The existence of precursors, i.e. local slip events before the onset of sliding, has been verified experimentally (Rubinstein et al., 2007; Maegawa et al., 2010; Katano et al., 2014) and captured by many numerical models (Bouchbinder et al., 2011; Kammer et al., 2012; Radiguet et al., 2013; Trømborg et al., 2014; Taloni et al., 2015; Roch et al., 2022). The propagation of wavefronts with different velocities has also been observed both in experiments (Rubinstein et al., 2004; Xia et al., 2004; Coker et al., 2005; Ben-David et al., 2010) and in simulations (Braun et al., 2009; Trømborg et al., 2011; Bar-Sinai et al., 2013; Amundsen et al., 2015; Trømborg et al., 2015; Svetlizky et al., 2016), and analogies with fracture mechanics have been highlighted and exploited to quantitatively investigate this aspect of frictional phenomena (Barras et al., 2020; Svetlizky and Fineberg, 2014; Thøgersen et al., 2014; Kammer et al., 2015).

On nominally flat surfaces, the regions where slip precursors occur is influenced by the tangential driving force: in Rubinstein et al. (2007) they were observed at the trailing edge and their length, i.e. the their propagation distance, has been predicted by means of fracture mechanics models (Kammer et al., 2015; Bayart et al., 2016). The frequency of these precursors, which redistribute the surface stress in a non-uniform way and induce a change of the contact area, grows until a macroscopic rupture front nucleates and propagates along the whole surface. The emergent static global friction properties, i.e. the first maximum load level reached by the total tangential force in a sliding test, is largely determined by these effects, as recently shown in Gvirtzman and Fineberg (2021).

These studies are important not only to increase our understanding of basic friction phenomena taking place at the interface between solids, but also for applications in biology and Labonte et al. (2014), Filippov and Gorb (2016) and Tramsen et al. (2018), in engineering and materials science (Etsion, 2004; Gachot et al., 2017; Rosenkranz

* Corresponding author at: Laboratory for Bioinspired, Bionic, Nano, Meta Materials & Mechanics, Department of Civil, Environmental and Mechanical Engineering, University of Trento, Via Mesiano 77, 38123 Trento, Italy.
E-mail addresses: gianluca.costagliola@epfl.ch (G. Costagliola), federico.bosia@polito.it (F. Bosia), nicola.pugno@unitn.it (N.M. Pugno).

https://doi.org/10.1016/j.ijsolstr.2022.111525
Received 1 July 2021; Received in revised form 7 December 2021; Accepted 15 February 2022
Available online 26 February 2022

et al., 2019), and in geophysics, to interpret the signals recorded during the preparatory phase preceding an earthquake (Dieterich, 1978; Rice, 1993; Lapusta and Rice, 2003; Bar Sinai et al., 2012; Lambert et al., 2021).

This body of literature demonstrates the importance of studying slip precursors and the dynamics underlying stress redistribution before and during the transition to sliding. However, the understanding of these phenomena is often complicated by the presence of multiple length scales at the interfaces. Thus, it is crucial to investigate how the interplay between length scales affects the formation and propagation of slip precursors.

In Costagliola et al. (2018), we investigated how the macroscopic static friction coefficient is affected by two-dimensional surface structures, which give rise to these non-trivial phenomena. We observed a non monotonic behavior of the static friction coefficient with the surface length scales and non linear effects for anisotropic shapes. Moreover, we showed that the global static friction is not only determined by the non-uniform tangential stress distribution before the sliding phase, but also by the dynamics of the transition, i.e. the propagation of the slip front. An example of this is the case of a patterned surface with straight narrow grooves. This configuration has been analyzed numerically and experimentally in the literature, in particular in the case of laser textured surfaces (Prodanov et al., 2013; Gachot et al., 2013; Rosenkranz et al., 2014; Gnilitskyi et al., 2019), demonstrating that patterning reduces friction, but with a non-trivial dependence on system geometric parameters. In our study, considering an elastic patterned surface over a rigid flat substrate, we have found that static friction is greater when the grooves are perpendicular to the sliding direction rather than parallel to it. However, the tangential stress on the edges before sliding is larger in the former case, so that we would expect a smaller static friction. This apparent paradox is explained by the subsequent dynamic evolution. When the motion begins, grooves aligned with the sliding direction favor the rupture front propagation, so that the global tangential force peak is smaller. This example illustrates how the stress redistribution after every local slip event is fundamental to understand how a surface structure modifies the onset of dynamic motion.

In this paper, we further investigate these concepts from a more general point of view. We focus on determining the localization of slip precursors and the propagation of the rupture waves, which determine the emergent static friction properties. Due to the stress concentrations on the edges of surface patterns, during the rupture process there is a time sequence of localized slip precursors leading to the sliding of the whole contact region. The length scale of the patterns has a non-trivial interplay with the occurrence and location of slip precursors, with different regimes in which the transition from a static to a dynamic phase, from sharp becomes smooth. We show how the interplay between slip precursors and two geometric length scales affect the macroscopic sliding event. We deal with this problem by means of numerical simulations using the two-dimensional spring-block model introduced in Costagliola et al. (2018), allowing to take into account simultaneously longitudinal and tangential stress on the edges of surface features.

The paper is organized as follows: in Section 2 we present the model. In Section 3.1, we consider the case of non-patterned surfaces, to clarify the general dynamic of the model and to obtain benchmark results. In Section 3.2 we consider square pillar patterns to explain the interplay between the pattern length scale and the slip precursors. In Section 3.3, we introduce the hierarchical patterning and in Sections 4 and 5 we provide the discussion and conclusions.

2. Model

We adopt the formulation of the spring-block model introduced in Costagliola et al. (2018), considering an elastic material sliding over a non-deformable rigid substrate. The elastic surface is discretized

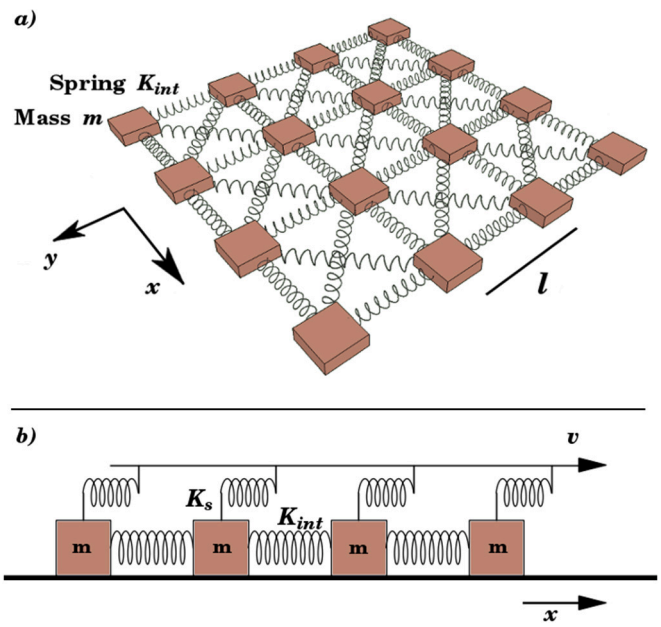

Fig. 1. (a) Discretization of a square surface into a 2-D spring-bock model, showing the mesh of the internal springs K_{int}. The shear springs (K_s) attached above the blocks are not shown. (b) Side view showing the slider moving at constant velocity v and the shear springs.

into elements of mass m, each connected by springs to the eight first neighbors and arranged in a regular square mesh (Fig. 1a) with N_x (N_y) blocks along the $x(y)$ axis at a distance $l_x(l_y)$. In order to obtain the equivalence of this spring–mass system with a homogeneous elastic material of Young's modulus E, the Poisson's ratio is fixed to $\nu = 1/3$ (Absi and Prager, 1975), $l_x = l_y \equiv l$ and $K_{int} = 3/4El_z$, where l_z is the thickness of the 2-D layer and K_{int} is the stiffness of the springs connecting the four nearest neighbors of each block, i.e. those aligned with the axes. The stiffness of the diagonal springs must be $K_{int}/2$.

The internal elastic force on the block i exerted by the neighbor j is $\mathbf{F}^{(ij)}_{int} = k_{ij}(r_{ij} - l_{ij})(\mathbf{r}_j - \mathbf{r}_i)/r_{ij}$, where $\mathbf{r}_i$, $\mathbf{r}_j$ are the position vectors of the two blocks, r_{ij} is the modulus of their distance, l_{ij} is the modulus of the rest distance and k_{ij} is the stiffness of the spring connecting them.

All the blocks are connected by springs of stiffness K_s to the slider that is moving at constant velocity v in the x direction (Fig. 1b). Hence, the shear force exerted by the slider on the block i is $\mathbf{F}^{(i)}_s = K_s(\mathbf{v}t + \mathbf{r}^0_i - \mathbf{r}_i)$, where $\mathbf{r}^0_i$ is the initial rest position of the block and $\mathbf{v} = (v, 0)$ is the slider velocity vector. The total driving force on i can be defined as $\mathbf{F}^{(i)}_{mot} = \sum_j \mathbf{F}^{(ij)}_{int} + \mathbf{F}^{(i)}_s$. The stiffness K_s can be expressed as a function of the macroscopic shear modulus $G = 3/8E$, so that by simple calculations we obtain $K_s = K_{int}l^2/l_z^2$. In the following, for simplicity we fix $l_z = l$. Thus, the elementary mass is $m = \rho l^3$, where ρ is the material density. Moreover, we consider only a square mesh, i.e. $N_x = N_y \equiv N$.

In the spring-block model, a viscous damping force, proportional to the velocity, is added to eliminate artificial block oscillations, i.e. $\mathbf{F}^{(i)}_d = -\gamma m\dot{\mathbf{r}}_i$, where $\gamma = 5\ \mathrm{ms}^{-1}$ is the damping frequency.

The interaction with the substrate is modeled as described in Costagliola et al. (2018, 2016), i.e. as an Amontons–Coulomb friction force with a statistical distribution on the friction coefficients: while the block i is at rest, the friction force $\mathbf{F}^{(i)}_{fr}$ opposes the total driving force, i.e. $\mathbf{F}^{(i)}_{fr} = -\mathbf{F}^{(i)}_{mot}$, up to a threshold value $F^{(i)}_{fr} = \mu_{si}\ F^{(i)}_n$, where μ_{si} is the static friction coefficient and $F^{(i)}_n$ is the normal force on i. When this limit is exceeded, a constant dynamic friction force opposes the motion, i.e. $\mathbf{F}^{(i)}_{fr} = -\mu_{di}\ F^{(i)}_n \hat{\mathbf{r}}_i$, where μ_{di} is the dynamic friction coefficient and $\hat{\mathbf{r}}_i$ is the velocity direction of the block. Given the applied pressure

P, the normal force $F_n^{(i)}$ can be calculated as $F_n^{(i)} = Pl^2$ and the total normal force is $F_n = Pl^2N^2$.

In the following, we will drop the subscript s, d every time the considerations apply to both the coefficients. The microscopic friction coefficients are extracted from a Gaussian statistical distribution to account for the randomness of the surface asperities, i.e. $p(\mu_i) = (\sqrt{2\pi}\sigma)^{-1} \exp[-(\mu_i - (\mu)_m)^2/(2\sigma^2)]$, where $(\mu)_m$ denotes the mean of the microscopic friction coefficients and σ is its standard deviation. The mean microscopic static and dynamic friction coefficients are fixed conventionally to $(\mu_s)_m = 1.0(1)$ and $(\mu_d)_m = 0.60(5)$, respectively, where the numbers in brackets denote the standard deviations of their Gaussian distributions.

Thus, the Newton's law for the block i is: $m\ddot{\mathbf{r}}_i = \sum_j \mathbf{F}_{int}^{(ij)} + \mathbf{F}_s^{(i)} + \mathbf{F}_{fr}^{(i)} + \mathbf{F}_d^{(i)}$. The overall system of differential equations is solved using a fourth-order Runge–Kutta algorithm. In order to calculate the average of any observable, the simulation must be repeated various times, extracting each time new random friction coefficients. In repeated tests, an integration time step $h = 10^{-8}$ s proves to be sufficient to reduce integration errors under the statistical uncertainty in the range adopted for the parameters of the system.

The global emergent friction force can be calculated from the sum of the longitudinal forces exerted by the slider, i.e. $F_{fr} = |\sum_i \mathbf{F}_s^{(i)}|$, which corresponds to the longitudinal friction force that would be measured in an experiment of linear sliding.

Realistic values are chosen for the physical system parameters, i.e. a Young's modulus $E = 10$ MPa, which is typical for a soft polymer or rubber-like material, a density $\rho = 1.2$ g/cm^3, and a normal pressure $P = 0.05$ MPa. We have chosen these values as an average of those used in previous experimental work on these systems (Balestra et al., 2022; Berardo et al., 2019), but we note that, in the spring-block model, the relevant parameters is the ratio between Young's modulus and applied pressure, so that our results are qualitatively the same for all larger Young's moduli, provided that the pressure is also increased. The slider velocity is $v = 0.05$ cm/s, similar to those adopted in recent experiments with surface textures (Berardo et al., 2019; Sahli et al., 2018; Maegawa et al., 2016). The distance between blocks l in the model is an arbitrary parameter representing the smallest surface feature that can be modeled and is chosen by default as $l = 10^{-3}$ cm.

For discussion on the effect of these approximations, the comparison with other formulations of the literature, and the choices of parameters, we refer the reader to Costagliola et al. (2018). We remark here that the formulation is appropriate to describe the transition to sliding for slow velocities, assuming a constant real contact area and neglecting any long-term dynamical effects. For this reason, it is more effective in estimating the values of the static friction coefficient with respect to the dynamic ones (Berardo et al., 2019). Moreover, the current setup cannot capture phenomena related to the vertical stress distributions (Guarino et al., 2018) or wave propagation in the bulk, and those related to the modification of the real contact area (Balestra et al., 2022; Sahli et al., 2018). Nevertheless, the model is able to provide a good qualitative understanding at the onset of sliding at relatively small computational costs with respect to other full three-dimensional methods.

In order to simulate the presence of patterning on the surface, we set to zero the friction coefficients of the blocks located in correspondence with detached regions from the rigid plane. These blocks are not considered in contact with the ground, and the total normal force is distributed only on contact blocks. This is a good approximation to find the in-plane stress distribution at least for shallow structures, i.e. when their length along the vertical axis is larger than surface roughness, but sufficiently small to avoid significant effects due to the vertical shear stress, like deformation, tilting or bending of these structures. In Berardo et al. (2019), in which surface structures fulfill this condition, this model is able to reproduce the qualitative trends of the static friction coefficients by varying the structure length.

3. Results

3.1. Non-patterned surface

As discussed in Costagliola et al. (2018), our formulation of the spring-block model (for a non-patterned surface) provides a qualitative description of the onset of the sliding motion. In the following, we will refer to detachment of a single block to indicate its transition from static to dynamic friction.

The typical time evolution of the total friction force is shown in Fig. 2. Slip precursors occur as single detachment events before the macroscopic sliding phase, corresponding to the weakest microscopic static friction thresholds. From these events,macroscopic rupture waves may nucleate. Parameters like the slider velocity, pressure, or statistical distributions of the local friction coefficients all affect the number of wave fronts, but in any case the time instant t_{max} at which the maximum tangential force occurs and the global static coefficient is calculated, corresponds to the onset of propagation. Once the detachment fronts have traveled across the whole contact surface, a non-uniform distribution of residual strains appears at the time instant corresponding to the relative minimum of the force after the first peak in Fig. 2. These residual strains are removed at the beginning of the dynamic phase (Radiguet et al., 2013), when localized stick–slip motions of small fractions of the contact area take place.

Fig. 2 displays the corresponding number of blocks detaching over time: the precursors are those occurring before t_{max}, whereas after this time instant there is the main sliding avalanche, highlighted by the peak of the number of detachments. The two peaks are clearly separated: t_{max} occurs before the average detachment time calculated over all blocks, namely t_{avg}, which corresponds roughly to the propagation instant of the wave fronts over the whole surface. The time sequence of detachments on the two-dimensional surface is graphically illustrated in Fig. 3. From this we observe that not all the precursors trigger a rupture wave front.

3.2. Single-scale patterned surfaces

On non-patterned surfaces, the localization of slip precursors and nucleation points are determined by the statistical distributions of the local friction coefficients. Thus, on average, each point of the surface has the same probability of being a nucleation point, and in repeated simulations the spatial distribution on the surface of the initial detachment time is uniform. This situation changes in the presence of surface patterning. Here, we consider square pillars, which are a simple configuration to investigate these effects from a qualitative point of view.

In order to simulate these structures, we set to zero the local friction coefficients of the blocks not corresponding to the pillar regions. We indicates with l_p and l_s the pillar size and spacing, respectively, which can be normalized by the elementary block distance l, so that we can define $n_p \equiv l_p/l$ and $n_s \equiv l_s/l$ corresponding to the pillar and spacing length expressed in terms of number of blocks. Fig. 4 shows an example of a surface portion characterized by equally spaced square pillars.

The distance between surface edges and the pillars close to them is $l_s/2$ to reduce boundary effects. We have verified in preliminary tests that, with this choice, all the pillars have the same average statistical properties and are subject to the same stress distributions for $n_p \geq 4$. The case $n_p \leq 3$ is peculiar, since the number of blocks on the pillar is too small to induce a non-trivial stress distribution. In this case, the transition to sliding is similar to that for a non-patterned surface, so that in the following analysis we restrict to the cases $n_p \geq 4$.

The non-uniform surface stress distribution occurring on the surface of a single pillar before sliding induces a specific detachment time sequence, as shown in Fig. 5. First, regions on the corners detach, then those on the boundaries perpendicular to the sliding direction, followed by those on the parallel boundaries. This is because the longitudinal

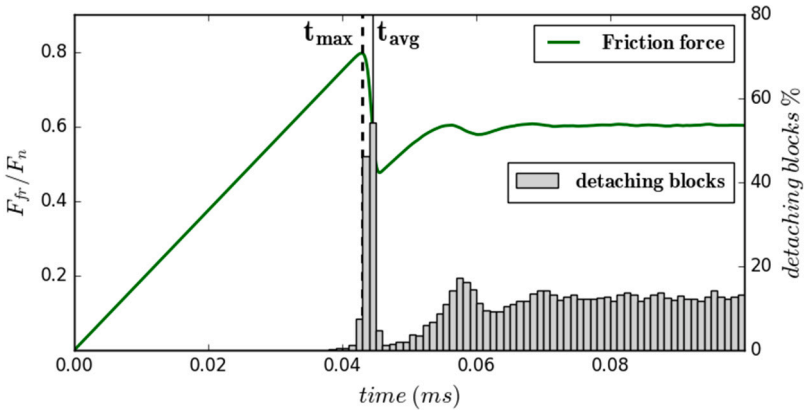

Fig. 2. Time evolution for the total friction force and percentage of detaching blocks, i.e. blocks switching from static to dynamic friction in small time ranges, for a non-patterned surface. The vertical dotted line marks the maximum of the total friction force, occurring at t_{max} and the thin solid line the average detachment time t_{avg}. Slip precursors appear before t_{max}, while the global detachment event occurs shortly after it. This simulation is performed with default parameter values and $N = 120$.

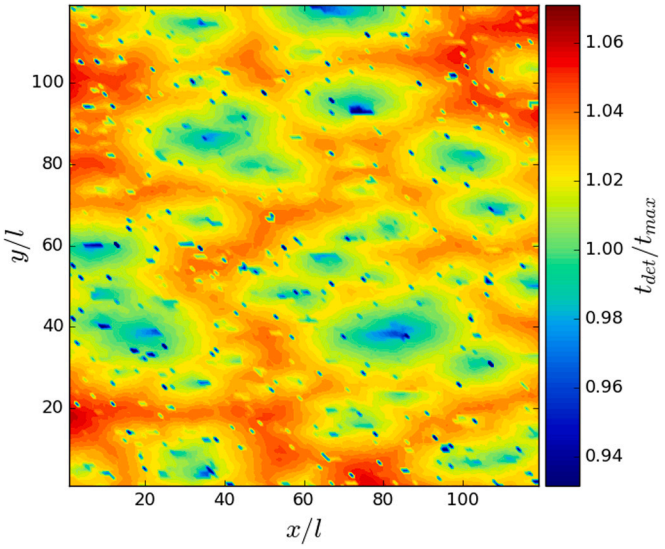

Fig. 3. Color map of the times t_{det} of the first detachment of the blocks on the surface, corresponding to the time evolution of Fig. 2. Times are normalized with respect to t_{max}, so that blue corresponds to detachment before the force peak and the red to those after that. The slip precursors appear as dark blue spots, not all of which give rise to a detachment nucleation point, e.g. those located in red regions.

stress exerted on orthogonal edges is larger than in-plane shear stress along parallel ones. This sequence is repeated for the blocks adjacent to those on the borders. These detachments occur before the maximum of the friction force is reached and the global sliding begins, so that they can be considered sliding precursors. Finally, detachment waves are triggered from nucleation points located near the edge and propagate towards the central part of the pillar, which is the last part detaching. The number of wave fronts crossing the pillar and the exact location of the nucleation points is influenced by the random distribution of the local friction coefficients, but the described detachment sequence always occurs, independently of statistical properties.

The sequence reflects the initial stress distribution and its redistribution after the first detachments, but the macroscopic consequence is the inversion between t_{max} and t_{avg}, i.e. the force peak always occurs after the average detachment time. This implies that the sliding precursors are not only a few isolated blocks, but a whole region localized around the edge of the pillar. This is a qualitative change of the dynamics occurring at the onset of sliding motion, which is reflected in the shape of the force time evolution curve that is no longer a sharp peak, and becomes rounded.

This can be observed in Fig. 6, which illustrates the time evolution of the force and the number of detachments for various values of n_p. While for $n_p = 2$ the behavior is similar to a non-patterned surface, for $n_p \geq 6$ the sliding precursors are numerically relevant and occur for a larger time interval before t_{max}. For very large pillars, e.g. $n_p = 60$, the static friction coefficient increases again and the transition is sharper. This is because the region characterized by sliding precursors, localized around the edges of the pillars, becomes negligible with respect to the surface area of the central part, which is involved in the main detachment front after the time t_{max}.

The characteristic length of the slip precursors on the pillar sides in orthogonal directions is not symmetric due to the preferential sliding direction. This asymmetric behavior has been observed in recent experiments (Sahli et al., 2018). In the 2-D spring-block model, this causes different detachment processes at orthogonal sides of the pillar.

If τ_1, τ_2 are the detachment times of two points x_1 and x_2 located on the same pillar side, we can calculate the time correlation function $C(x_1, x_2) \equiv \langle \tau_1 \tau_2 \rangle - \langle \tau_1 \rangle \langle \tau_2 \rangle$, where $\langle ... \rangle$ denotes the average over repeated simulations. If the correlation is zero, the detachment times in repeated simulations are uncorrelated. This implies that, despite τ_1, τ_2 have the same average value, they detach independently of each other. Instead, in the presence of correlation, their detachment could be triggered by the same precursor events involving more blocks. The precursor length can be estimated as the distance over which a significant correlation exists.

In Fig. 7, we report the correlation function calculated from the central point of each side as a function of the distance along the same side. In symbols, on sides along x, the time correlation function are calculated between the points $x_1 = (n_p/2, 0)$ and $x_2 = (np/2 + r, 0)$ as $c_x(r) \equiv C(x_1, x_2)/C(x_1, x_1)$, which is the normalized correlation function. The same definition applies for the side along y between the points $y_1 = (0, n_p/2)$ and $y_2 = (0, np/2 + r)$, with $c_y(r) \equiv C(y_1, y_2)/C(y_1, y_1)$. These correlation functions are shown in Fig. 7 for various r values: while $c_y(r)$ decreases rapidly, $c_x(r)$ displays a correlation over a wide range of values. From this, we deduce that on sides aligned with the sliding direction slip precursors have a non-negligible characteristic correlation length. Although edges parallel to the sliding direction detach slightly after the perpendicular ones, their slip involves a larger number of blocks.

The correlation functions decreases exponentially, i.e. $c_x(r) \sim e^{-r/l_c}$, where l_c is the characteristic correlation length, which can be estimated by fitting the correlation functions. In the inset of Fig. 7, we report the fit results for l_c for various pillar sizes n_p, obtained by averaging the correlation functions. It is difficult to estimate l_c for $n_p \lesssim 10$ since there are few blocks to fit, however we can deduce that $l_c/l \gtrsim 3$ and that it is slightly increasing with n_p.

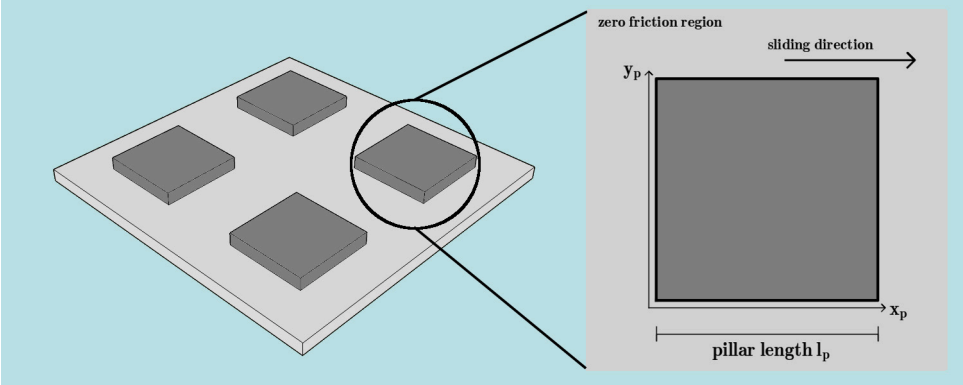

Fig. 4. Surface patterning using square pillars. A single pillar is highlighted in the enlargement with the coordinates of its points (x_p, y_p) adopted in the next plots.

This means that when the characteristic correlation length is comparable to the total length of the pillars, a slip precursor can lead to the detachment of the whole side of the pillar, leading to a faster detachment process and a globally smaller static friction. This explains why the smallest static friction is obtained for an specific intermediate value of n_p, as can be observed in Fig. 6, and the force peak at the transition is considerably more rounded.

Thus, this formulation of the spring-block model predicts an optimal length scale of the pillars which maximizes the occurrence of sliding precursors, so that the static friction is minimized and the transition to sliding is facilitated. One could argue that this feature is inherent to the discretization length of the model. However, this minimum value for intermediate sizes of the pattern is also observed in experimental results (Murarash et al., 2011; Li et al., 2016; Berardo et al., 2019). In real systems, there is a characteristic length scale of the precursors (Kammer et al., 2015; Bayart et al., 2016) which must be taken into account and compared to the length scale of the patterns. When the precursor length scale is greater or much smaller than the pattern size, the transition is qualitatively similar to that of a non-patterned surfaces, although the effective emergent value of the static friction coefficient can be different due to the different stress distributions. In the intermediate regime, i.e. for precursor length scales comparable to the pattern size, the slip precursors involve a relevant fraction of the contact surface and the detachments are distributed over a longer time interval around the maximum of the friction force. This leads to a longer duration of the transition between static and dynamic friction.

3.3. Multiscale patterned surfaces

Next, we consider the case in which the patterning geometry (i.e. the square pillars discussed in Section 3.2) is split into smaller substructures, giving rise to the presence of two different length scales in the patterning structure. The simplest structure to consider is a pillar characterized by high-aspect ratio longitudinal or transversal grooves, as shown in Fig. 8. We simulate these configurations again by setting to zero the friction coefficients of blocks corresponding to the grooves. We adopt the same notation of Section 3.2, i.e. a point on a pillar is denoted with its coordinates (x_p, y_p). Length and spacing of the first level pillar are denoted with $l_p^{(1)}$ and $l_s^{(1)}$, respectively. The structure sizes of the second-level, in this case pawls and grooves, are denoted with $l_p^{(2)}$ and $l_s^{(2)}$, respectively. Any length l_i with a generic subscript i can be normalized by the elementary length $n_i \equiv l_i/l$.

This type of multiscale (hierarchical) configuration combines the effects analyzed in the previous section due to the precursors appearing along the sliding direction, with another characteristic length due to the second level structures. As observed in Costagliola et al. (2016) and Brely et al. (2018), a hierarchical configuration allows to distribute mechanical stresses more uniformly over the surface and, in this case,

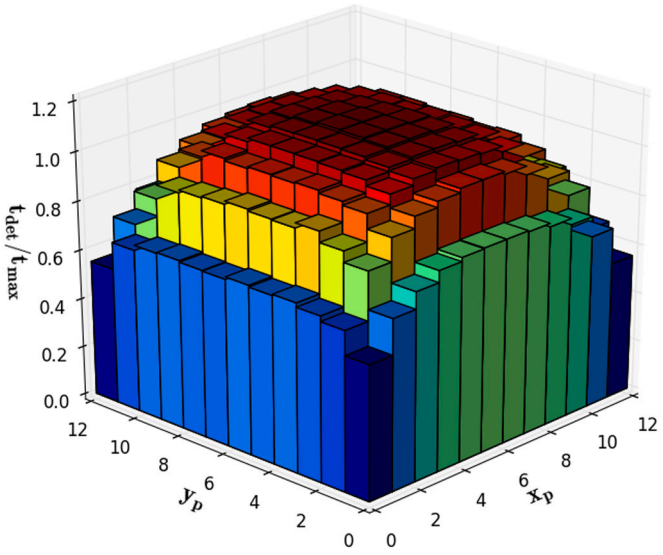

Fig. 5. Average first-detachment time t_{det} (normalized with respect to t_{max}) of the blocks on a single pillar of size $n_p = 20$.

increases the total effective length of the edges, i.e. the regions giving rise to slip precursors. Thus, there is a precise rupture time sequence as in the single-level patterns, starting from blocks located on the transversal side of the pillar, followed by those on the longitudinal external one. Shortly after these, there is the detachment of the blocks located along the longitudinal internal sides, i.e. along the second level grooves. The last stage of detachment takes place in the internal regions of the pawls.

In the time evolution of the longitudinal friction force, the transition from static to dynamic friction is characterized by two load peaks separated by an intermediate quasi-static phase (see Fig. 9). The geometry of these configurations divides the contact surface into two parts of equal size with distinct dynamics: the edge regions where slip precursors originate, and the internal core of the contact structures. The external edges of the pillars are subjected to larger longitudinal stresses than the internal ones along the second-level grooves. For this reason, the former detach before the latter, but the correlation functions along the longitudinal edges display the same qualitative shape shown in Section 3.2. The typical correlation length is also the same. Thus, all the edges along the second-level grooves are characterized by slip precursor with non-negligible length. This leads to a faster detachment of the boundary regions and, consequently, to the first load peak.

The time interval between the first and the second peak is controlled by the difference between the length scales. The global static friction,

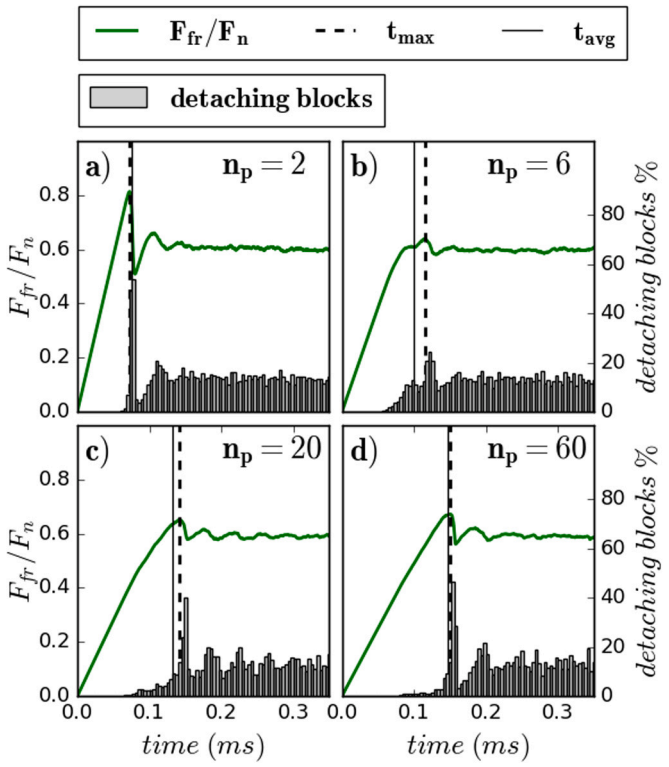

Fig. 6. Time evolution of the friction force and block detachments for various n_p values. In the case $n_p = 2$, the dynamics of the transition to sliding is similar to that of non-patterned surfaces, while in the other cases the detachment sequence described in Section 3.2 occurs.

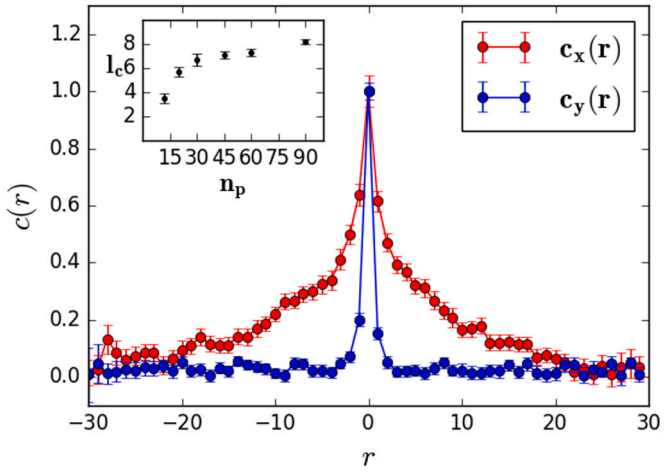

Fig. 7. Time correlation functions $c_x(r)$ and $c_y(r)$ on orthogonal sides of the pillar for the case $n_p = 60$. A point located on a pillar is identified by its coordinates as defined in Fig. 4 $x = (x_p, y_p)$. On the side aligned with the sliding direction x, the points are $x_1 = (n_p/2, 0)$ and $x_2 = (n_p/2 + r, 0)$, and $c_x(r) \equiv C(x_1, x_2)/C(x_1, x_1)$. On the side along y, the points are $y_1 = (0, n_p/2)$ and $y_2 = (0, n_p/2 + r)$, and $c_y(r) \equiv C(y_1, y_2)/C(y_1, y_1)$. In the inset, the estimates of the characteristic correlation length l_c as a function of the pillar size n_p obtained through the fit of $c_x(r) \sim e^{-r/l_c}$.

which is determined by the force reached at the second load peak, can be manipulated by modifying the pillar length $l_p^{(1)}$, although in general all the factors analyzed in Costagliola et al. (2018) must be considered.

The two load peaks appear only if the second level grooves are aligned with the sliding directions. On the contrary, if the sliding direction is along the y-axis, most of the precursors are uncorrelated so that there is no large detachment determining the first load peak observed in Fig. 9. Thus, this effect is due to two fundamental factors: the concurrent presence of multiple characteristic length scales, $l_s^{(2)} \ll l_s^{(1)}$ (hierarchical structure), and the anisotropic shape of the second-level grooves exploiting the occurrence of slip precursors with non-negligible length along the longitudinal edges.

The results obtained for a simple two-level structure can be generalized to multiple length scales and more complex geometries or to other surface patterns, provided that a hierarchical organization is present. Hierarchy is necessary but not sufficient, since the shape of the surface patterns and the alignment with the sliding direction must be designed to maximize the occurrence of precursor length. An anisotropic shape, similar to that of the second-level patterns considered here, is another fundamental factor to obtain such non-trivial frictional behaviors. We expect that these effects remain present when adding further hierarchical levels, although other physical mechanisms should be considered beyond the current model at smaller length scales.

4. Discussion and relevance to seismic phenomena

The non-trivial behavior described in the previous section could be exploited in applications involving patterned surfaces for friction control, e.g., whenever a rapid transition from static to dynamic friction is required while maintaining a smooth force behavior. In the phase between load peaks such as those appearing in Fig. 9, the system is in a static friction phase, since the internal regions of the patterning are still at rest, while the regions involved by precursors events undergo a stick–slip motion after the first detachment. However, the whole contact surface is in a stressed state, involving a combination of inhomogeneous stress and partial detachment, which can lead to full detachment in the presence of a small additional force. These effects could also be relevant for understanding the tribology of structured surfaces, including in biological systems. For example, in recent years, the pre-stressed state of the gecko paw has been investigated and identified as one of the key factors responsible for its capability to detach easily despite its strong static adhesion (Chen et al., 2009).

Additionally, the results discussed in this paper are consistent with a large body of seismic data and could provide elements for its better understanding and interpretation. Starting from the seminal paper by Dieterich (1978), earthquake precursors have been linked to preseismic fault creep and correlated to geometric dimensions of earthquake source zones. Preseismic slip has been found to be an intrinsic part of the process of homogenization of stress along a fault leading to unstable (seismic) slip (Papadimitriou, 2008). Precursor activity has been identified as one of the key ingredients in the field of earthquake prediction (Sykes, 1996), with much discussion on whether the probability for large earthquake occurrence is highest during time periods of smaller event activation or quiescence (Rundle et al., 2011).

Analysis of seismic data sets has highlighted the presence of a complex nucleation phase, characterized by slip events distributed over long times (Linde et al., 1988; Bouchon et al., 2011, 2013; Hasegawa and Yoshida, 2013) and sequences of localized precursor events have been observed (Ellsworth and Beroza, 1995; Dodge et al., 1996; Schaff et al., 2002). Similar conclusions have also been obtained from rigorous earthquake models involving sliding faults governed by rate and state friction laws (Lapusta and Rice, 2003; Lapusta et al., 2000). The relevance of slip precursors to characterize and possibly to predict macroscopic events has also been highlighted by discrete element models (Ferdowsi et al., 2013) and by spring-block models (Brown et al., 1991; Mori and Kawamura, 2008b,a).

Our analysis introduces the possibility of correlating the observed phenomenology of seismic events to the geometrical features of the corresponding fault regions, possibly characterizing them statistically. In

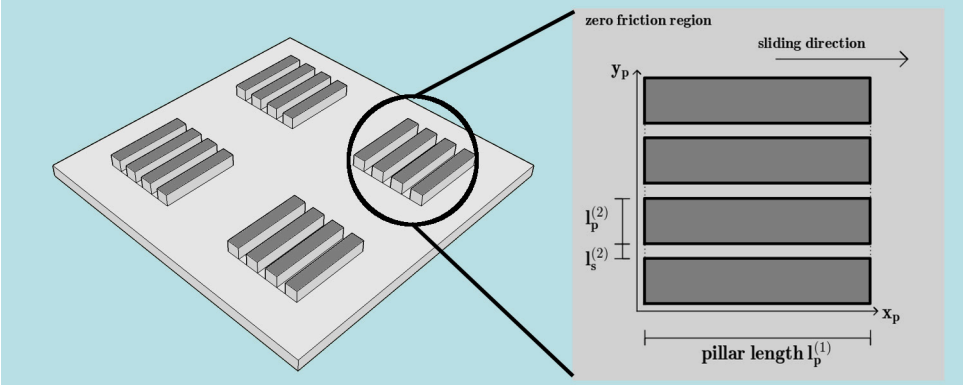

Fig. 8. Second level hierarchical patterning with high aspect ratio structures. In the enlargement, a single first level single pillar and second level structures in the adopted coordinate system.

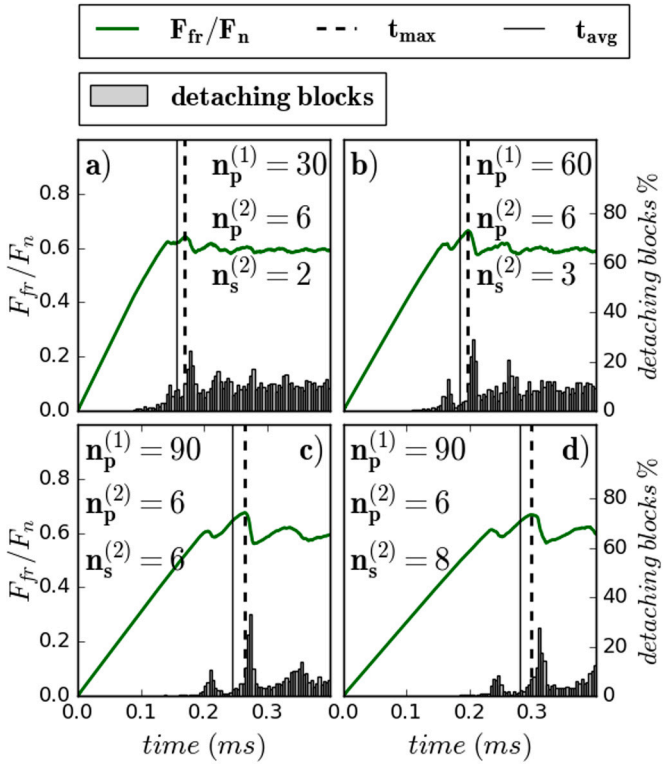

Fig. 9. Time evolution of the friction force and block detachment for various hierarchical configurations. The transition from static to dynamic friction is characterized by a double peak, corresponding to the distinct detachments of boundary and central regions of the structures.

particular, according to our analysis, the presence of an extended precursor phase could be correlated to multiscale fault geometry, involving characteristic length scales of which the fundamental one is expected to be of the order of the precursor correlation lengths. Our analysis on the effects of multiscale hierarchical geometrical features are consistent with studies on the implications on earthquake nucleation of geometric irregularity of the rupturing surfaces in fault lines (Ohnaka and Shen, 1999), including when the geometry involves multiscale heterogeneity (Aochi and Ide, 2017). Our results also indicate that an extended precursor phase is linked to the presence of pre-existing faults with inhomogeneous stress distributions, reflecting the fact that stress transfer and stress triggering phenomena have been invoked in the past for the onset of seismic activity (Stein et al., 1994). Specific aspects related to the application of our model to seismic problems will be the focus of future work.

5. Conclusions

Using a 2-D spring-block model we have investigated the transition from static to dynamic friction in the presence of hierarchical multiscale surface structures. The occurrence of slip precursors and how they affect the global emergent behavior have been discussed. In the case of nominally flat surfaces, isolated precursor events occur before global detachment, leading to the nucleation of a macroscopic rupture front, whose propagation over the whole surface marks the peak of the global static friction force.

In the presence of surface patterns, non-uniform surface stress distributions before sliding lead to different detachment sequences, and the macroscopic rupture wave is preceded by multiple precursor events originating from the edges of the structures. A characteristic length emerges, which can be estimated from the time correlation function, affecting the global transition to sliding: when the patterning size and the length of the precursors are of the same order, static friction is smaller and the transition load peak becomes smoothed.

In the presence of multiple scale levels in the patterning, the effect is replicated at all size scales, leading to a detachment phase characterized by multiple distinct peaks, between which the surface is in a static friction condition but also in a stressed state, allowing a rapid but smooth transition to sliding. We show that this complex behavior emerges in the presence of both multiscale and appropriate anisotropic features in the surface patterning, and present a specific example of surface texture with these characteristics. Various other types of surface patterns could be designed to tune the specific behavior in the transition to sliding. These could be exploited to optimize the frictional properties of artificial devices switching continuously from static to dynamic sliding. Moreover, the discussed mechanisms could be responsible for the observed phenomenology in seismic precursor events and could be helpful in predicting earthquake events, based on the deduced average stress state of the involved fault lines.

Declaration of competing interest

The authors declare that they have no known competing financial interests or personal relationships that could have appeared to influence the work reported in this paper.

Acknowledgments

FB and NMP are supported by the European Commission under the FET Open "Boheme" grant no. 863179. GC has received funding from the European union's Horizon 2020 research and innovation programme under the Marie Sklodowska-Curie grant agreement no. 754462. The authors acknowledge the Province of Trento for the financial support provided with the LP 6/99 for the "Meta-F" project. Computational resources were provided by hpc@polito (http://www.hpc.polito.it) and by the Centro di Competenza sul Calcolo Scientifico (C3S) of the University of Torino (c3s.unito.it)

References

Absi, E., Prager, W., 1975. Comparison of equivalence and finite element methods. Comput. Methods Appl. Mech. Eng. 6, 59.

Amundsen, D.S., Trømborg, J., Thøgersen, K., Katzav, E., Malthe-Sørenssen, A., Scheibert, J., 2015. Steady-state propagation speed of rupture fronts along one-dimensional frictional interfaces. Phys. Rev. E 92, 032406.

Aochi, H., Ide, S., 2017. Role of multiscale heterogeneity in fault slip from quasi-static numerical simulations. Earth Planets Space 69, 94.

Balestra, S., Costagliola, G., Pegoraro, A., Picollo, F., Molinari, J.-F., Pugno, N.M., Vittone, E., Bosia, F., Sin, A., 2022. Experimental and numerical study of the effect of surface patterning on the frictional properties of polymer surfaces. J. Tribol. 144, 031704.

Bar Sinai, Y., Brener, E.A., Bouchbinder, E., 2012. Slow rupture of frictional interfaces. Geophys. Res. Lett. 39, L03308.

Bar-Sinai, Y., Spatschek, R., Brener, E., Bouchbinder, E., 2013. Instabilities at frictional interfaces: Creep patches, nucleation, and rupture fronts. Phys. Rev. E. 88, 060403.

Barras, F., Aldam, M., Roch, T., Brener, E.A., Bouchbinder, E., Molinari, J.-F., 2020. The emergence of crack-like behavior of frictional rupture: Edge singularity and energy balance. Earth Planet. Sci. Lett. 531, 115978.

Bayart, E., Svetlizky, I., Fineberg, J., 2016. Fracture mechanics determine the lengths of interface ruptures that mediate frictional motion. Nat. Phys. 12.

Ben-David, O., Cohen, G., Fineberg, J., 2010. The dynamics of the onset of frictional slip. Science 330, 211.

Berardo, A., Costagliola, G., Ghio, S., Boscardin, M., Bosia, F., Pugno, N.M., 2019. An experimental-numerical study of the adhesive static and dynamic friction of micropatterned soft polymer surfaces. Mater. Des. 181, 107930.

Bouchbinder, E., Brener, E.A., Barel, I., Urbakh, M., 2011. Slow cracklike dynamics at the onset of frictional sliding. Phys. Rev. Lett. 107, 235501.

Bouchon, M., Durand, V., Marsan, D., Karabulut, H., J., S., 2013. The long precursory phase of most large interplate earthquakes. Nat. Geosci. 6, 299.

Bouchon, M., Karabulut, H., Aktar, M., Ozalaybey, S., Schmittbuhl, J., Bouin, M., 2011. Extended nucleation of the 1999 Mw 7.6 izmit earthquake. Science 331, 877.

Braun, O.M., Barel, I., Urbakh, M., 2009. Dynamics of transition from static to kinetic friction. Phys. Rev. Lett. 103, 194301.

Brely, L., Bosia, F., Pugno, N.M., 2018. Emergence of the interplay between hierarchy and contact splitting in biological adhesion highlighted through a hierarchical shear lag model. Soft Matter 14, 5509.

Brown, S.R., Scholz, C.H., Rundle, J.B., 1991. A simplified spring-block model of earthquakes. Geophys. Res. Lett. 18, 215.

Chen, B., Wu, P., Gao, H., 2009. Pre-tension generates strongly reversible adhesion of a spatula pad on substrate. J. R. Soc. Interface 6, 529.

Coker, D., Lykotrafitis, G., Needleman, A., Rosakis, A.J., 2005. Frictional sliding modes along an interface between identical elastic plates subject to shear impact loading. J. Mech. Phys. Solids 53, 884.

Costagliola, G., Bosia, F., Pugno, N.M., 2016. Static and dynamic friction of hierarchical surfaces. Phys. Rev. E 94, 063003.

Costagliola, G., Bosia, F., Pugno, N.M., 2018. A 2-D model for friction of complex anisotropic surfaces. J. Mech. Phys. Solids 112, 50.

Dieterich, J.H., 1978. Preseismic fault slip and earthquake prediction. J. Geophys. Res. 83, 3940.

Dodge, D.A., Beroza, G.C., Ellsworth, W.L., 1996. Detailed observations of california foreshock sequences: implications for the earthquake initiation process. J. Geophys. Res. 101, 371.

Ellsworth, W.L., Beroza, G.C., 1995. Seismic evidence for an earthquake nucleation phase. Science 268, 851.

Etsion, I., 2004. Improving tribological performance of mechanical components by laser surface texturing. Tribol. Lett. 17, 733.

Ferdowsi, B., Griffa, M., Guyer, R.A., Johnson, P.A., Marone, C., Carmeliet, J., 2013. Microslips as precursors of large slip events in the stick-slip dynamics of sheared granular layers: A discrete element model analysis. Geophys. Res. Lett. 40, 4194.

Filippov, A., Gorb, S.N., 2016. Modelling of the frictional behaviour of the snake skin covered by anisotropic surface nanostructures. Sci. Rep. 6, 23539.

Gachot, C., A., R., Hsu, S.M., Costa, H., 2017. A critical assessment of surface texturing for friction and wear improvement. Wear 372, 21.

Gachot, C., Rosenkranz, A., Reinert, L., Ramos-Moore, E., Souza, N., Muser, M., Muklich, F., 2013. Dry friction between laser-patterned surfaces: Role of alignment, structural wavelength and surface chemistry. Tribol. Lett. 49, 193.

Gnilitskyi, I., Rota, A., Gualtieri, E., Valeri, S., Orazi, L., 2019. Tribological properties of high-speed uniform femtosecond laser patterning on stainless steel. Lubricants 7, 83.

Guarino, R., Costagliola, G., Bosia, F., Pugno, N.M., 2018. Evidence of friction reduction in laterally graded materials. Beil. J. Nanotechnol. 9, 2443.

Gvirtzman, S., Fineberg, J., 2021. Nucleation fronts ignite the interface rupture that initiates frictional motion. Nat. Phys. 17, 1037.

Hasegawa, A., Yoshida, K., 2013. Preceding seismic activity and slow slip events in the source area of the 2011 Mw 9.0 Tohoku-Oki earthquake: a review. Geosci. Lett. 2, 6.

Kammer, J., Radiguet, M., Ampuero, J., Molinari, J.F., 2015. Linear elastic fracture mechanics predicts the propagation distance of frictional slip. Tribol. Lett. 57, 23.

Kammer, D.S., Yastrebov, V.A., Spijker, P., Molinari, J.F., 2012. On the propagation of slip fronts at frictional interfaces. Tribol. Lett. 48, 27.

Katano, Y., Nakano, K., Otsuki, K., Matsukawa, H., 2014. Novel friction law for the static friction force based on local precursor slipping. Sci. Rep. 4, 6324.

Labonte, D., Williams, J.A., Federle, W., 2014. Surface contact and design of fibrillar 'friction pads' in stick insects (Carausius morosus): mechanisms for large friction coefficients and negligible adhesion. J. R. Soc. Interface 11, 0034.

Lambert, L., Lapusta, N., Perry, S., 2021. Propagation of large earthquakes as self-healing pulses or mild cracks. Nature 591, 252.

Lapusta, N., Rice, J.R., 2003. Nucleation and early seismic propagation of small and large events in a crustal earthquake model. J. Geophys. Res. 108, 2205.

Lapusta, N., Rice, J.R., Ben-Zion, Y., Zheng, G., 2000. Elastodynamic analysis for slow tectonic loading with spontaneous rupture episodes on faults with rate- and state-dependent friction. J. Geophys. Res. 105, 765.

Li, N., Xu, E., Liu, Z., Wang, X., Liu, L., 2016. Tuning apparent friction coefficient by controlled patterning bulk metallic glasses surfaces. Sci. Rep. 6, 39388.

Linde, A.T., Suyehiro, K., Miura, S., Sacks, I.S., Takagi, A., 1988. Episodic aseismic earthquake precursors. Nature 334, 513.

Maegawa, S., Itoigawa, F., Nakamura, T., 2016. Effect of surface grooves on kinetic friction of a rubber slider. Tribol. Int. 102, 326.

Maegawa, S., Suzuki, A., Nakano, K., 2010. Precursors of global slip in a longitudinal line contact under non-uniform normal loading. Tribol. Lett. 38, 3.

Mori, T., Kawamura, H., 2008a. Simulation study of earthquakes based on the two-dimensional Burridge-Knopoff model with long-range interactions. Phys. Rev. E 77, 051123.

Mori, T., Kawamura, H., 2008b. Simulation study of the two-dimensional Burridge-Knopoff model of earthquakes. J. Geophys. Res. 113, B06301.

Murarash, B., Itovicha, Y., Varenberg, M., 2011. Tuning elastomer friction by hexagonal surface patterning. Soft Matters 7, 5553.

Ohnaka, N., Shen, L., 1999. Scaling of the shear rupture process from nucleation to dynamic propagation: Implications of geometric irregularity of the rupturing surfaces. J. Geophys. Res. 104, 817.

Papadimitriou, P., 2008. Identification of seismic precursors before large earthquakes:Decelerating and accelerating seismic patterns. J. Geophys. Res. 113, B04306.

Prodanov, N., Gachot, C., Rosenkranz, A., Muklich, F., Muser, M., 2013. Contact mechanics of laser-textured surfaces. Tribol. Lett. 50, 41.

Radiguet, M., Kammer, D.S., Gillet, P., Molinari, J.F., 2013. Survival of heterogeneous stress distributions created by precursory slip at frictional interfaces. Phys. Rev. Lett. 111, 164302.

Rice, J.R., 1993. Spatio-temporal complexity of slip on a fault. J. Geophys. Res. 98, 9885.

Roch, T., Brener, E.A., Molinari, J.-F., Bouchbinder, E., 2022. Velocity-driven frictional sliding: Coarsening and steady-state pulses. J. Mech. Phys. Solids 158, 104607.

Rosenkranz, A., Grutzmacher, P.G., Gachot, C., Costa, H.L., 2019. Surface texturing in machine elements - A critical discussion for rolling and sliding contacts. Adv. Eng. Mater. 21, 1900194.

Rosenkranz, A., Reinert, L., Gachot, C., Mücklich, F., 2014. Alignment and wear debris effects between laser-patterned steel surfaces under dry sliding conditions. Wear 318, 49.

Rubinstein, S.M., Cohen, G., Fineberg, J., 2004. Detachment fronts and the onset of dynamic friction. Nature 430, 1005.

Rubinstein, S.M., Cohen, G., Fineberg, J., 2007. Dynamics of precursors to frictional sliding. Phys. Rev. Lett. 98, 226103.

Rundle, J.B., Holliday, J.R., Yoder, M., Sachs, M.K., Donnellan, A., Turcotte, D.L., Tiampo, K.F., Klein, W., Kellogg, L.H., 2011. Earthquake precursors: activation or quiescence? Geophys. J. Int. 187, 225.

Sahli, R., Pallares, G., Ducottet, C., Ben Ali, I.E., Al Akhrass, S., Guibert, M., Scheibert, J., 2018. Evolution of real contact area under shear and the value of static friction of soft materials. Proc. Natl. Acad. Sci. 115, 471.

Schaff, D.P., Bokelmann, G.H.R., Beroza, G.C., Waldhauser, F., Ellsworth, W.L., 2002. High-resolution image of Calaveras fault seismicity. J. Geophys. Res. 107, 2186.

Stein, R.S., King, G.C.P., Lin, J., 1994. Stress triggering of the 1994 M=6.7 Northridge, California, earthquake by its predecessor. Science 265, 1432.

Svetlizky, I., Fineberg, J., 2014. Classical shear cracks drive the onset of dry frictional motion. Nature 509, 205.

Svetlizky, I., Pino Munoz, D., Radiguet, M., Kammer, D.S., Molinari, J.F., J., F., 2016. Properties of the shear stress peak radiated ahead of rapidly accelerating rupture fronts that mediate frictional slip. Proc. Natl. Acad. Sci. 113, 542–547.

Sykes, L.R., 1996. Intermediate- and long-term earthquake prediction. Proc. Natl. Acad. Sci. 93, 3732.

Taloni, A., Benassi, A., Sandfeld, S., Zapperi, S., 2015. Scalar model for frictional precursors dynamics. Sci. Rep. 5, 8086.

Thøgersen, K., Trømborg, J., Sveinsson, H.A., Malthe-Sørenssen, A., Scheibert, J., 2014. History-dependent friction and slow slip from time-dependent microscopic junction laws studied in a statistical framework. Phys. Rev. E 89, 052401.

Tramsen, H.T., Gorb, S.N., Zhang, H., Manoonpong, P., Dai, Z., Heepe, L., 2018. Inversion of friction anisotropy in a bio-inspired asymmetrically structured surface. J. R. Soc. Interface 15, 2017062.

Trømborg, J., Scheibert, J., Amundsen, D.S., Thøgersen, K., Malthe-Sørenssen, A., 2011. Transition from static to kinetic friction: Insights from a 2D model. Phys. Rev. Lett. 107, 074301.

Trømborg, J., Sveinsson, H., Scheibert, J., Thøgersen, K., Malthe-Sørenssen, A., Amundsen, D., 2014. Slow slip and the transition from fast to slow fronts in the rupture of frictional interfaces. Proc. Natl. Acad. Sci. 111, 8764.

Trømborg, J., Sveinsson, H.A., Thøgersen, K., Scheibert, J., Malthe-Sørenssen, A., 2015. Speed of fast and slow rupture fronts along frictional interfaces. Phys. Rev. E 92, 012408.

Xia, K., Rosakis, A.J., Kanamori, H., 2004. Laboratory earthquakes: the sub-Rayleigh-to-supershear rupture transition. Science 303, 1859.